Visible and 1.54 μm Emission From Amorphous Silicon Nitride Films by Reactive Cosputtering

Selçuk Yerci, *Student Member, IEEE*, Rui Li, Sergei O. Kucheyev, Tony van Buuren,
Soumendra N. Basu, and Luca Dal Negro

(Invited Paper)

***Abstract*—In this paper, we present our main results on the structural and optical properties of light-emitting amorphous silicon nitride (SiN_x) films fabricated by reactive magnetron cosputtering. In particular, we discuss the origin of the visible emission in amorphous silicon nitride films and investigate the optical emission properties of Erbium-doped amorphous silicon nitride (Er:SiN_x). The mechanisms of Er excitation and de-excitation in Er:SiN_x are discussed in relation to the engineering of efficient light sources at 1.54 μm for on-chip nanophotonics applications. These results suggest that Er-doped amorphous silicon nitride films have a large potential for the fabrication of optically active photonic devices based on the Si technology.**

***Index Terms*—Amorphous semiconductors, erbium, photoluminescence, silicon alloys.**

I. INTRODUCTION

SILICON photonics can potentially provide the ultimate solution for the cost-effective integration of electronic and optical technologies on the same chip. The "missing link" in silicon photonics has long been the development of efficient light-emitting devices and silicon-based lasers [1]–[3]. The engineering of optical devices in silicon (Si), particularly light emitters and Si-based lasers atop the inexpensive silicon electronics platform, has the potential to revolutionize the optoelectronics industry by providing a definitive solution to the heat dissipation and interconnect bottleneck problems, which threaten the continued advance of highly integrated Si technology [1]–[3]. The convergence of optical technologies with the mature Si platform is expected to extend the reach of integrated optics into diverse fields, including low-cost, high-performance applications ranging from interchip to intrachip interconnects and communication to optical bio-sensing and integrated biochips for medical diagnostics. However, the progress toward these important goals has been limited so far due to the lack of efficient light emission from Si [1]–[4].

Photon emission from Si originates from low-probability phonon-mediated transitions that compete unfavorably with much faster nonradiative de-excitation processes, particularly Auger and free-carrier recombinations. In order to overcome these limitations, several successful strategies have been recently developed by many authors [5]–[11]. In particular, the approach of quantum confinement in Si nanostructures has led to substantial advancements in Si light emission efficiency, and it has sparked a race toward the demonstration of the first silicon-based laser [1], [6], [8], [9], [12]. This quest has recently led to an impressive development in the areas of light-emitting devices and stimulated Raman lasers [6], [10]–[14], optical modulators and switches [15], [16], Si-compatible detectors and sensors [17], photonic crystal structures and high-Q Si resonators [18], [19].

Among the different approaches developed to engineer on-chip Si-based light sources, rare earth doping of silicon-nanostructures can provide an effective solution at 1.54 μm, which is the ideal wavelength for planar Si integration. This approach hinges on the recent discovery of efficient energy transfer between Si nanocrystals (Si-ncs) in SiO_2 and Erbium (Er) ions [20]–[24], which has resulted in almost a three orders of magnitude larger Er excitation cross sections compared to Er-doped glasses.

Recently, Er-doped Si-rich Nitride (Er:SRN) materials have also been investigated as novel optical platforms for Si-based photonics applications. Similar to Er-doped oxides, Er:SRN show intense 1.54 μm photoluminescence (PL), small PL thermal quenching, and are ideally suited for the fabrication of high-quality photonic structures and electrically pumped devices [19], [25]–[36]. In this material, Er excitation occurs via a non-resonant, broadband, and nanosecond-fast energy transfer processes involving a high-density of small (2 nm) Si nanoclusters formed by thermal annealing [25]–[30]. On the other hand, efficient 1.54 μm emission with millisecond-long lifetime and nonresonant Er excitation have also been recently demonstrated, in the absence of Si nanocrystals, in Er-doped amorphous silicon

---

Manuscript received May 17, 2009; revised August 9, 2009. First published October 20, 2009; current version published February 5, 2010. This work was supported in part by the United States Air Force Multidisciplinary University Research Initiative program on "electrically pumped silicon-based lasers for chip-scale nanophotonic systems" supervised by Dr. G. Pomrenke. The work at Lawrence Livermore National Laboratory (LLNL) was performed under the auspices of the United States Department of Energy by LLNL under Contract DE-AC52-07NA27344.

S. Yerci and R. Li are with the Department of Electrical and Computer Engineering and Photonics Center, Boston University, Boston, MA 02215 USA (e-mail: syerci@bu.edu; ruili@bu.edu).

S. O. Kucheyev and T. van Buuren are with the Lawrence Livermore National Laboratory, Livermore, CA 94551 USA (e-mail: kucheyev@llnl.gov; vanbuuren1@llnl.gov).

S. N. Basu is with the Division of Materials Science and Engineering, Boston University, Brookline, MA 02446 USA, and also with the Department of Mechanical Engineering, Boston University, Boston, MA 02215 USA (e-mail: basu@bu.edu).

L. Dal Negro is with the Department of Electrical and Computer Engineering and Photonics Center, Boston University, Boston, MA 02215 USA, and also with the Division of Materials Science and Engineering, Boston University, Boston MA 02215 (e-mail: dalnegro@bu.edu).

Color versions of one or more of the figures in this paper are available online at http://ieeexplore.ieee.org.

Digital Object Identifier 10.1109/JSTQE.2009.2032516

nitride (Er:SiN$_x$) films fabricated by reactive cosputtering [34], [35]. Compared with both Si-rich oxide and SRN materials containing Si nanocrystals with 2–3 nm diameters, Er-doped SiN$_x$ (Er:SiN$_x$) films are characterized by a more homogeneous microstructure which could play an important role for the engineering of low-loss resonant photonic structures with controlled refractive indices in the 2.0–2.5 range and with reduced free carrier losses at 1.54 μm. However, little is known about the excitation/de-excitation mechanism of the 1.54 μm Er emission in these materials.

In this paper, we discuss in detail, the structural and optical properties of amorphous silicon nitride films (SiN$_x$) fabricated by reactive cosputtering. In particular, we discuss the origin of visible light emission and energy transfer in Er-doped SiN$_x$ materials with different excess Si concentrations. Finally, we investigate the temperature quenching of the Er:SiN$_x$ emission and provide specific design rules for the engineering of light-emitting devices based on Er:SiN$_x$ materials.

The rest of the paper is organized as follows: in Section II, we discuss the fabrication and structural characterization of Er-doped and undoped SiN$_x$ samples by reactive cosputtering. In Section III, we discuss the optical absorption and emission properties of SiN$_x$ films in the visible spectral range. In Section IV, we discuss the energy transfer process between the SiN$_x$ matrix and Er ions while in Section V, we consider the thermal quenching of the Er emission and its excitation/de-excitation processes. The influence of Si concentration and annealing temperature on the 1.54 μm Er emission is also discussed. Finally, the conclusions are presented in Section VI.

II. MATERIAL FABRICATION AND STRUCTURAL CHARACTERIZATION

Silicon nitride samples with various stoichiometries (SiN$_x$) can be fabricated by a variety of different techniques including N$_2$ reactive sputtering using a Si target, direct cosputtering using Si and Si$_3$N$_4$ targets, or chemical vapor deposition (CVD) methods such as low-pressure CVD and plasma-enhanced CVD with SiH$_4$ and N$_2$/NH$_3$/N$_2$O precursors. Direct cosputtering methods from Si$_3$N$_4$ and Si targets are less suitable for the deposition of SiN$_x$ films with low excess Si. SiN$_x$ samples deposited by CVD methods contain substantial amount of H, which leads to a detrimental absorption peak around 1.54 μm due to the formation of N–H bonds.

On the other hand, reactive sputtering deposition of SiN$_x$ films has the ability to deposit almost H and O free material over a large range of controlled stoichiometries ($0 < x < 1.33$). In addition, Er doping can easily be obtained by utilizing an Er target during the reactive sputtering.

In this study, SiN$_x$ and Er:SiN$_x$ films with different Si concentrations (Er:SiN$_x$ $x \leq 1.33$) were fabricated by N$_2$ reactive magnetron cosputtering using Si and Er targets in a Denton Discovery 18 confocal-target sputtering system. The relative concentrations of Si and N atoms in the samples were controlled by varying the N$_2$/Ar gas flow ratio. Post deposition annealing processes were performed in a rapid thermal annealing furnace at temperatures between 600 and 1150 °C, respectively for 200 s under forming gas (5% H$_2$, 95% N$_2$) to obtain the optimum Er PL intensity and lifetime for samples with different Si concentrations.

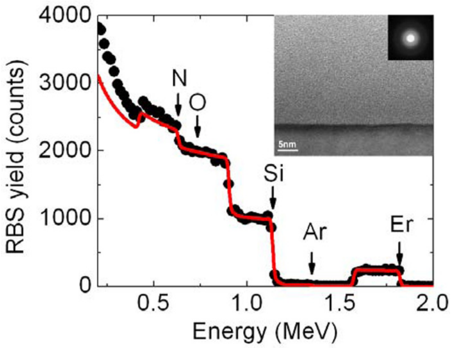

Fig. 1. Experimental RBS spectrum (points) and a RUMP simulation curve (solid line) for a 320-nm-thick Si = 48.0 at.%, N = 50.9 at.%, Er = 0.5 at.%, and Ar = 0.6 at.% film on a Si substrate. For clarity, only every fifth experimental point is shown. Surface peaks of Er, Ar, Si, O, and N are indicated by arrows. (Inset) HRTEM microimage and SAED pattern of the same sample.

The quantification of Si, N, and Er atoms in the matrix is crucial to understand the nature of the PL in these materials as well as to optimize the PL intensity and lifetime of Er. In this paper, Rutherford back scattering (RBS) was used to quantify the Er, Si, and N atoms with an accuracy of 0.7% for Si and N; 0.01% for Er. Depth profiles of Si, N, and Er atoms were studied by RBS with 2 MeV ^{4}He ions incident along the direction normal to the sample surface and backscattered to 164°. The analysis of the RBS spectra was performed with stopping powers and scattering cross sections from the RUMP code [37] assuming constant atomic density (9.53×10^{22} atoms/cm^3) and a layer composition of SiN$_x$Er$_y$.

In order to investigate the microstructure of the films, we performed high resolution transmission electron microscopy (HRTEM) studies in cross section using a JEOL 2010 operated at 200 kV, with a point-to-point resolution of 0.19 nm. Selected area electron diffraction (SAED) studies of the films in cross section were also performed to investigate the structure of the samples and the possible nucleation of Si nanocrystals or amorphous nanoclusters in Si-rich samples. Fourier transform infrared spectroscopy (FTIR) measurements were performed in transmission mode by Bruker IFS 66v/S to characterize the chemical environment and the degree of structural disorder in the films, which were deposited on a double side polished, high resistivity Si substrate.

The experimental RBS spectrum and a RUMP simulation curve for an Er:SiN$_x$ film with 6% excess Si are shown in Fig. 1. The HRTEM micrograph and SAED pattern of the same sample, annealed at 1150 °C for 200 s, are shown in the inset of Fig. 1. Both the HRTEM and the SAED analysis demonstrate an amorphous film structure with no evidence of Si nanocrystals. This is in contrast with the microstructure of Si-rich nitride films with comparable refractive indices fabricated by direct magnetron cosputtering, which result in the nucleation of small Si nanocrystals when annealed within the same temperature range [30]. However, it is important to note that our HRTEM analysis cannot exclude the formation of very small amorphous

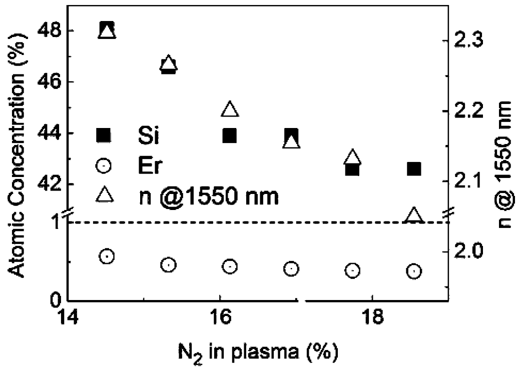

Fig. 2. Relative atomic concentrations of Si (solid squares), Er (open circles) and refractive index (n) values at 1550 nm in the films as a function of N_2 flow rate%. The dashed line indicates the atomic concentration is equal to 1%.

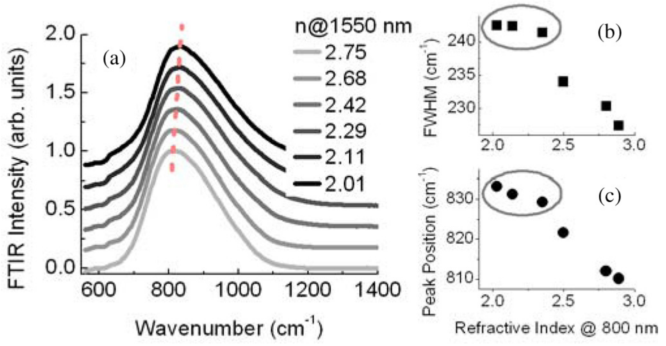

Fig. 3. (a) FTIR spectra of ~350 nm thick the samples with various Si concentrations (b) and (c) are the variations of the FWHM and peak position of the Si–N stretching band with excess Si, respectively.

Si clusters in the films, which is consistent with the existence of a two phase system, amorphous Si and SiN$_x$, as observed by X-ray absorption and emission studies on the same samples [38].

The relation between the relative Si concentration and refractive index measured at 1550 nm is shown in Fig. 2. The refractive indices of the films tend to increase linearly with the Si concentration in the measured range.

In Fig. 2, we also show the relative atomic concentrations of Si and Er atoms in the films as a function of the percentage of nitrogen gas flow rate (N_2 flow rate%) to the total gas rate. We have found that by decreasing the N_2 flow rate% the nitrogen atomic concentration in the films decreases while both the Si and Er (Fig. 2) concentrations increase. This is because more Ar ions are available to sputter Si and Er atoms at small N_2 flow rate%, limiting Si reactions and forming Si-rich (substoichiometric) films. The RBS analysis demonstrated a homogenous distribution of Er ions throughout the films (see Fig. 1) with concentrations varying between 3.7×10^{20} and 4.7×10^{20} Er/cm^3 for all the samples.

The chemical environment and the Si–N vibrational structure of the samples were investigated by FTIR spectroscopy. The peak position and full width at half maximum (FWHM) of the Si–N stretching band were monitored to investigate the strength of the bonds and the structural disorder in the SiN$_x$ matrix. It is worth noting that FTIR analysis did not show evidence of H atoms in the films. The absence of H is very significant in Er-doped SiN$_x$ films since it enables the fabrication of low-loss waveguides and resonator structures at 1.54 μm [39]. Therefore, reactive sputtering is a suitable deposition method for the fabrication of SiN$_x$ materials for photonics applications.

In Fig. 3(a), we show the Si–N–Si stretching vibrational band of the SiN$_x$ films with various excess Si. The FWHM and the peak position of the Si–N stretching band decreases with the excess Si, as shown in Fig. 3(b) and (c), respectively. The FWHM of the Si–N band correlates with the degree of the disorder in the SiN$_x$ matrix [40], which increases with the incorporation of N_2 in the films [41], [42]. It should be noted that the data points for the samples showing the best light emission intensity (encircled in Fig. 3) exhibit only a very small dependence on the excess Si in the films. The variation of the Si–N peak position, which is related to the strength of the Si–N bond, is also shown in Fig. 3. The peak position of the FTIR spectrum shifts to higher energies with N_2 incorporation, although this shift is very limited compared to SiO$_x$ materials due to the more rigid SiN$_x$ bond structure [40]. It is important to notice that the best emitting samples (encircled) share similar Si–N peak positions. These results demonstrate that strong bond interactions and a high degree of structural disorder are directly involved in the optical emission of SiN$_x$ films.

III. MECHANISM OF VISIBLE EMISSION FROM SiN$_x$

In order to understand the origin of the visible light emission in SiN$_x$ films, which is important for the engineering of the 1.54 μm Er emission in Er:SiN$_x$, we performed optical transmission, ellipsometry, steady-state PL and time-resolved PL (TRPL) studies for SiN$_x$ samples with varying Si concentrations.

Transmission measurements of SiN$_x$ and Er:SiN$_x$ films deposited on quartz substrates were performed between 200 and 1800 nm using a Cary 5000 double beam spectro-photometer. Additionally, the samples were analyzed using spectroscopic ellipsometry to obtain the thickness and optical constant. The Δ and Ψ values were measured using a J. A. Woollam Co. variable-angle spectroscopic ellipsometer in a spectral range 250–1800 nm. The data were analyzed using the Tauc–Lorentz and Cauchy–Urbach models [43]. The optical band gaps are calculated from the Tauc's plot using the relation $(\alpha h\nu)^{1/2} = \text{const.}(h\nu\text{-}E_{\text{Tauc}})$. The absorption coefficients $\alpha(\lambda)$ of the samples are calculated from the transmission and ellipsometry measurements. The normal incidence reflection of the films is estimated from the corresponding refractive indices according to the relation $R = \{(n-1)/(n+1)\}^2$.

Fig. 4 shows the Tauc plot for SiN$_x$ films with different excess Si concentrations. The Tauc optical gaps are dispersed within an energy range from ~3.0 to ~4.1 eV for the best emitting samples.

PL spectra were measured at room temperature using 100 fs pulses (82 MHz repetition rate) from the third harmonic of a Ti:sapphire laser (Mai Tai HP, Spectra Physics) at 288 nm. The quasi-steady-state excitation beam was modulated by a mechanical chopper and the PL emission was lock-in detected by

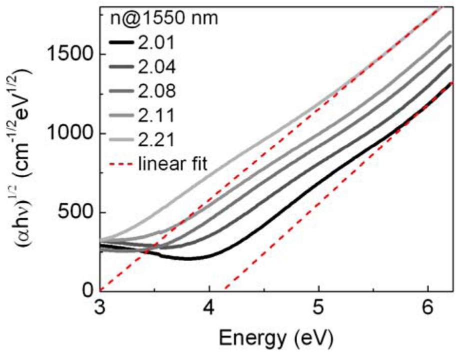

Fig. 4. Tauc plot of the ~80 nm think SiN$_x$ samples with different Si concentrations. The increase in the absorption at low energies is due to the interference of the light in the thin films.

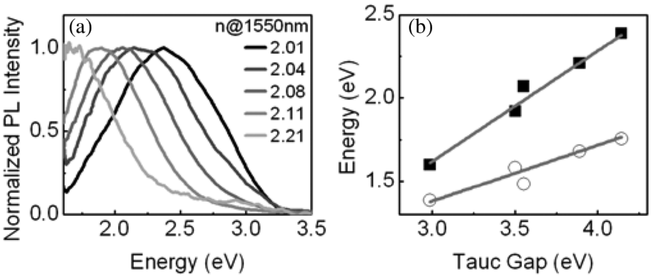

Fig. 5. (a) PL spectra of ~80 nm thick SiN$_x$ films. (b) Change of the PL peak position (closed squares) and the Stokes shift (open circles) as a function of the optical gap. The straight lines are the best linear fits to the data and shown as guide to the eye.

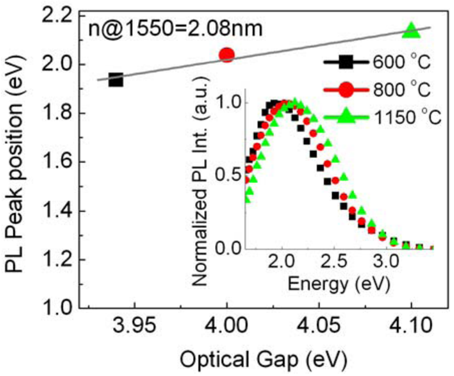

Fig. 6. Change of the PL peak position with Tauc optical gap for samples annealed at 600 (squares), 800 (circles), and 1150 °C (triangles). The straight line is plotted to guide the eye. PL spectra of the same samples are given in the inset. The sample thickness was 76 nm.

a photomultiplier tube (Oriel 77348). Fig. 5(a) shows the PL spectra for SiN$_x$ films with different Si concentrations. We observe that the peak positions of the almost Gaussian PL spectra can be tuned from ~1.6 to 2.4 eV by decreasing the excess Si in the SiN$_x$. Although this trend appears to be in agreement with the standard quantum confinement explanation where more excess Si results in the nucleation of larger Si-ncs with lower emission energies, we reemphasize that we have not observed the nucleation of Si-ncs in our films by HRTEM analysis. As already noted in Section II, this is a remarkable material difference with respect to SiN$_x$ films by direct cosputtering, where the nucleation of small-size Si-ncs and the absence of PL band tuneability have been previously demonstrated and attributed to surface-trapped exciton recombination [25], [27]–[29]. The different microstructure of the reactively sputtered amorphous SiN$_x$ films presented in this paper is, therefore, conducive to a different light emission mechanism.

It has been proposed that localized states in the band tails of amorphous Si-based alloys can result in widely tunable and visible light emission [41], [44]–[48]. According to studies [41], [42], [44], [47], [48], visible light emission can originate from the radiative recombination of photo-generated carriers trapped at localized states by disorder-induced potential fluctuations within the exponential band tails of the amorphous material. The photo-excited carriers first undergo a fast thermalization to the band edges and then initiate a slower thermalization in the band tails. The radiative recombination occurs when carriers reach the deepest tail states, so-called carrier-tail states, for which the radiative recombination and thermalization rates are approximately equal. This model assumes that band tail states are distributed randomly in space with exponential energy correlation [42], [44], [47], [48].

Fig. 5(b) shows the dependence of the PL peak position and of the Stokes shift, defined as the energy difference between absorption and emission edge, with the optical gap of the samples. The linear relation between the PL peak position and the optical gap indicates that the properties of absorption and emission in SiN$_x$ are directly related to the amount of excess Si. In particular, in amorphous materials, excess Si lowers the optical gap and, therefore, the energy difference of the states from the conduction and valence band tails, which explains the red-shift of the band-tail-related PL. On the other hand, the Stokes shift in these samples can be explained entirely due to the thermal relaxation of the carriers along the band tails [49]. As we know from FTIR, the addition of N atoms introduces more disorder in the SiN$_x$ amorphous system and widens the band tails, explaining the larger Stokes shifts observed for samples with larger optical gaps [42].

As shown in Fig. 6, the PL peak positions and the optical gaps shift to higher energy (blue-shift) with annealing temperature. This blue shift cannot be explained by quantum confinement models, in agreement with the HRTEM analysis that did not evidence the nucleation of nanocrystals in our films. Therefore, based on HRTEM and on the facts that both the PL peak position and the optical gap consistently shift to the blue with annealing temperature, we believe that localized states within the band tails of the amorphous SiN$_x$ materials are the origin of the observed PL. It is worth noting, here, that the PL intensity increases with annealing temperature up to approximately 1000 °C and then saturates or decreases depending on the Si concentration (data not shown here). The initial enhancement is attributed to the thermal passivation of defects such as Si dangling bonds in the matrix. The origin of the decrease after a certain temperature remains unclear, but it could originate from the formation of extrinsic defect centers due to excess Si in the films.

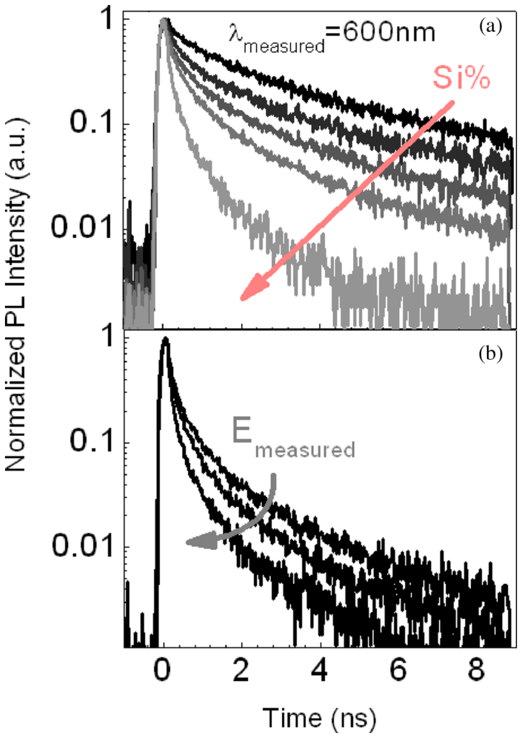

Fig. 7. (a) PL decay traces of the ∼80 nm thick samples with the refractive indices of 2.01, 2.04, 2.08, 2.11, and 2.21 measured at 1550 nm by spectroscopic ellipsometer. The arrow indicates the increasing Si concentration in the films. (b) PL decay traces of the samples with a refractive index of 2.31 measured at 1.55, 1.77, and 2.07 eV. The arrow indicates the increasing energies where PL data is collected.

In order to deepen our understanding of the PL mechanism we performed TRPL experiments under pulsed excitation. The samples were excited by the second harmonic of the Mai Tai laser at 430 nm with 100 fs pulses. The TRPL signal was dispersed through a double grating spectrometer (Acton Spectra Pro. 2300i) and detected using a single-photon counting streak camera with 10 ps time-resolution (Hamamatsu, C4770). As shown in Fig. 7(a), the PL lifetimes of the samples are of the order of a few nanoseconds, which is much shorter than the typical lifetimes observed in efficient-emitting Si nanocrystals embedded in silicon oxide (∼10–100 μs) [29]. Moreover, the PL lifetimes of the SiN$_x$ samples with higher Si concentrations are significantly shorter, as shown in Fig. 7(a). The measured PL lifetime of the Si-rich and stoichiometric SiN$_x$ samples are approximately 3 and 12 ns, respectively. The PL efficiency of the investigated SiN$_x$ films was found to decrease dramatically with Si concentration (data not shown here), suggesting an increase in the number of nonradiative centers with Si concentration. We emphasize again that, due to the different microstructure of the materials, this behavior is very different from previously reported data on cosputtered and plasma enhanced CVD grown Si-rich silicon nitrite films [25]–[30], where an optimum excess Si concentration exists for highest PL intensity.

In Fig. 7(b), we show the PL decay traces of the sample with a refractive index of 2.31 measured at 1.55, 1.77, and 2.07 eV. The longest component of the decay data were obtained by fitting the PL traces with three exponential decays convoluted with the system response, resulting in 3.0, 3.7, and 4.0 ns, respectively for corresponding energies. The distribution of the PL lifetimes with energy supports the localized states nature of the band tails emission in SiN$_x$ [42], [50]. The PL decay dynamics follows the density of states (DOS) of the amorphous system. Since the band tails are distributed exponentially in energy, the DOS is higher at higher energies where carriers are less localized and mostly recombine nonradiatively. The thermalization rate decreases when carriers approach the deepest states in the band tails where they can be strongly localized. The radiative recombination occurs preferentially from these states, as supported by the strong Stokes shift measured in these samples. It is also important to note that the strongly nonexponential PL decay (Fig. 7) gives an additional indication of the random distribution of trap states with different recombination times [41], [42].

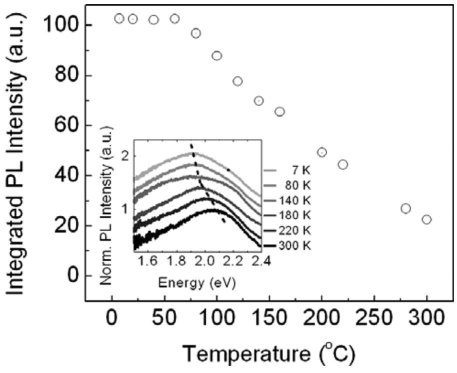

Fig. 8. Temperature dependence of the integrated PL intensity of the sample with a refractive index of 2.08 at 1550 nm. (Inset) Normalized PL spectra of the same sample measured at different temperatures. The sample is 340 nm thick.

Next, we investigated the thermal dependence of the PL spectra and intensity. Fig. 8 shows the quenching of the integrated PL intensity from SiN$_x$ sample measured from 7 to 300 K. The blue-shift of the PL peak position (Fig. 8, inset) and the decrease of PL intensity with temperature can be well explained by the recombination of carriers from higher energy states with increased nonradiative rates and reduced localization. The decrease and the gradual blue-shift of the PL emission peaks shown in the inset of Fig. 8 results directly from the recombination of photo-excited carriers which reached higher energy band-tail states as a result of thermal excitation. Therefore, since less localized, thermally activated carriers experience higher nonradiative recombination rates, they give rise to the temperature kinetics of the integrated PL emission shown in Fig. 8.

IV. ENERGY SENSITIZATION OF THE 1.54 μM ERBIUM EMISSION

The nature of the energy sensitization of Er emission at 1.54 μm has been extensively discussed in the literature of Si-ncs in SiO$_2$ matrices [20]–[22], [51], [52]. Here, we discuss the energy transfer mechanism from SiN$_x$ to Er ions. Steady-state room temperature and at cryogenic temperatures (down to 7 K) Er I_{PL} and τ_{PL} were excited nonresonantly using a 458 nm line of an Ar ion laser (Spectra Physics, 177–602) modulated

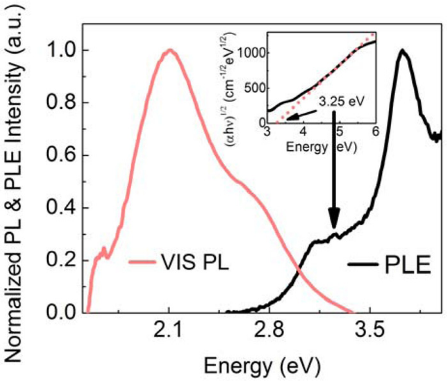

Fig. 9. Normalized visible PL and PLE (collected at 1.54 μm) spectra of the 360-nm thick stoichiometric sample ($n = 2.03$ at 1550 nm). The arrows point the energy of the optical gap calculated from the Tauc plot of the absorption data and linear fit as shown in the inset. The oscillatory behavior of the spectra is due to interference effects due to the film thickness.

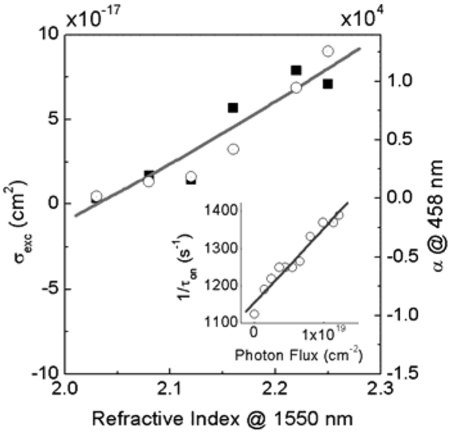

Fig. 10. Effective excitation cross sections $\sigma_{\rm eff}$ (squares) and the absorption coefficients α at 458 nm (circles) of the ~350 nm thick Er:SiN$_x$ samples with different excess Si%. The straight line is to guide the eye. (Inset) Linear fit of the experimental data of the difference between the reciprocal of the PL risetime and that of the PL lifetime to find the $\sigma_{\rm eff}$.

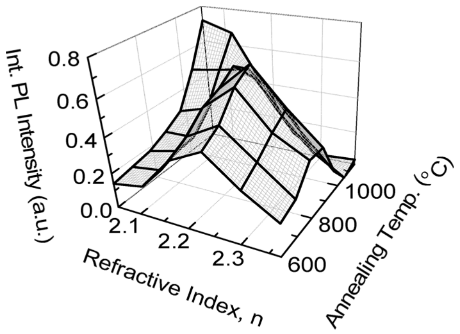

Fig. 11. Er integrated PL intensity of SiN$_x$ samples with various Si concentrations (refractive indices of the samples are measured at 1550 nm) annealed at temperatures of 600, 700, 800, 900, 1000, and 1150 °C. Samples are ~350 nm thick.

by a mechanical chopper and detected using either an InGaAs (Oriel 70368) or an extended photomultiplier tube (Hamamatsu R5509-73) detector attached to an oscilloscope. Additionally, we performed PL Excitation (PLE) measurements to study the spectral distribution of the Er excitation. A monochromatized Xe lamp was used as light source in PLE experiments. Moreover, from the Er PL lifetime ($\tau_{\rm PL}$) and risetime ($\tau_{\rm on}$) we measured the excitation cross section of Er ions at 458 nm.

The normalized PLE spectra collected at the 1.54 μm Er emission are shown in Fig. 9 for the Er-doped stoichiometric SiN$_x$ film which demonstrate that Er ions can be excited nonresonantly within a very broad spectral range [34], [53]. In addition, we have shown that the PLE spectra shift to longer wavelengths by increasing the Si concentration in the film (data not shown) [34], [44]. This behavior follows the red-shifts of the PL peak position and the optical band gap of SiN$_x$ with Si concentration. The inset of Fig. 9 shows the Tauc plot of the absorption data fitted to a linear model for the stoichiometric SiN$_x$ sample considered here. In Fig. 9, we also show the PL spectrum of the sample that demonstrates the large Stokes-shift due to the thermalization of the photo-excited carriers in the band tails followed by radiative recombination. Fig. 9 indicates that the energy sensitization of Er emission can occur at energies above and below the optical gap of the SiN$_x$ materials.

Although a microscopic picture is still lacking, our data demonstrates that disorder-induced localized states in SiN$_x$ can directly be involved in the energy transfer process to Er ions and result in 1.54 μm emission sensitization even below the SiN$_x$ optical absorption gap in the absence of Si nanocrystals.

We have further quantified the matrix-mediated Er excitation process by measuring the Er excitation cross section $\sigma_{\rm exc}$ for samples with different Si concentrations (Fig. 10). The parameter $\sigma_{\rm exc}$ can be directly measured in the weak excitation regime by the linear dependence of the Er PL rise time versus the pumping photon flux as shown in the inset of Fig. 10 [26], [30], [31], [54]. The measured $\sigma_{\rm exc}$ values at the 458 nm nonresonant Er excitation wavelength as a function of the refractive index of the films are shown in Fig. 10. The Er excitation cross section increases with the Si concentration in the films. Interestingly, the measured values of $\sigma_{\rm exc}$, which are in the 10^{-18}–10^{-16} cm^2 range, are similar to the values reported for Er-doped silicon nanocrystals embedded in silicon nitride and in silicon oxide matrices [26], [30], [31], [54]. We have additionally found that $\sigma_{\rm exc}$ and the measured absorption coefficient (from ellipsometry) at 458 nm show a similar trend with the Si concentration in the films. This suggests that the measured increase in $\sigma_{\rm exc}$ directly results from the enhanced absorption coefficient of Si-rich films.

V. OPTIMIZATION OF ERBIUM EMISSION IN SILICON NITRIDE

In this section, we present a systematic study of the optimization conditions for the sensitized Er emission in amorphous silicon-rich nitride films. The analysis is performed by measuring the 1.54 μm Er emission and decay time for a set of 42 samples with 7 different Si concentrations (refractive indices) and annealed a temperature range of 600–1150 °C. All the samples have been excited at 458 nm under identical pumping conditions and the results are shown in the Figs. 11 and 12. We notice from Fig. 11 that the Er PL intensities of samples with

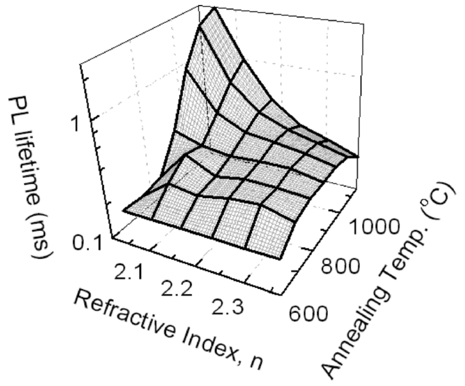

Fig. 12. Er PL lifetime of SiN$_x$ samples with various Si concentrations (refractive indices of the samples are measured at 1550 nm) annealed at temperatures of 600, 700, 800, 900, 1000, and 1150 °C. Samples are ∼350 nm thick.

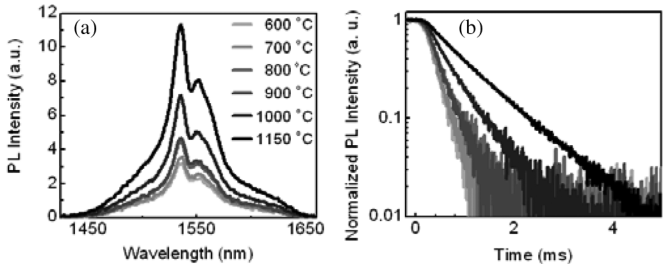

Fig. 13. (a) Er PL spectra of the 347 nm thick Er:SiN$_x$ sample with an excess Si 1.4% annealed at different temperatures. (b) Er PL decay traces of the same sample in (a).

high Si concentrations are optimized around 800–900 °C annealing temperatures, as previously reported [26]. However, we also indicate that similar PL intensities can be achieved across a large range of Si concentrations by annealing samples at different temperatures. In particular, the optimum 1.54 μm emission from samples with low Si concentrations requires the highest annealing temperatures. This behavior is clearly displayed in Fig. 13, which shows the PL spectra and PL decay traces of the samples with excess Si concentration of 1.4%. For the samples with excess Si concentration less than 1.4%, the PL intensities and lifetimes are the most intense and longest at the highest annealing temperature, 1150 °C. On the other hand, the annealing temperature should be lowered in samples with excess Si concentration above 1.4%.

The results in Fig. 12 demonstrate that the Er emission efficiency, which is proportional to the Er emission lifetime, is optimized for samples with the lowest Si concentration annealed at the highest temperatures [55]. In fact, the Er emission lifetime dramatically decreases by increasing the Si concentration in the films. Samples with almost an equilibrium stoichiometry (very low excess Si) and annealed at the highest temperatures (1150 °C) show the longest Er lifetime of ∼2.6 ms.

The data in Figs. 10–13 demonstrate the existence of a fundamental tradeoff between the Er excitation efficiency via energy transfer and the Er emission efficiency. Furthermore, an optimal annealing temperature exists for the Er emission in SiN$_x$ samples with different stoichiometries, pointing toward a complex interplay between the passivation of nonradiative defects in the matrix and the creation of extrinsic defect states associated to the incorporation of excess Si atoms in the SiN$_x$ matrix.

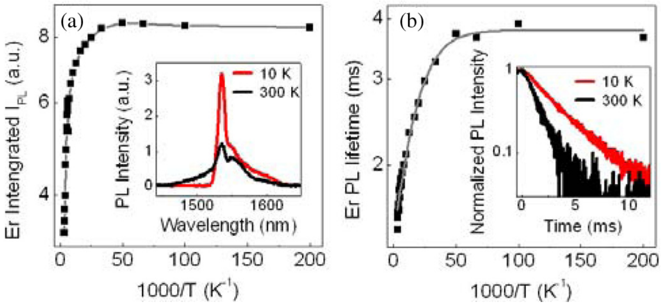

Fig. 14. Temperature dependence of (a) Er PL intensity and (b) Er PL lifetime at 1.54 μm of the Er-doped 340 nm thick stoichiometric SiN$_x$ sample ($n = 2.03$ at 1550 nm). Inset of (a) is the PL spectra of the sample at 10 and 300 K. Inset of (b) is the PL decay traces at 10 and 300 K.

In order to better understand the role of excess Si in the excitation/de-excitation processes in Er:SiN$_x$ matrices, we studied the temperature dependence of I_{PL} [Fig. 14(a)] and τ_{PL} [Fig. 14(b)] at both the Er and the SiN$_x$ (1.54 μm and from 0.5 to 0.8 μm depending on Si concentration). This allows us to investigate the nature of temperature quenching, determine the temperature dependence of the fundamental coupling parameter γ between Er ions and the SiN$_x$ matrix and discuss the mechanism of energy transfer in Er:SiN$_x$.

The PL lifetime of Er is subjected to the effect of nonradiative channels more directly than the PL intensity. Thus, we investigate first the temperature dependence of Er PL lifetime in Er:SiN$_x$. Fig. 14(b) shows the Er PL lifetimes τ_{PL} at 1.54μm as a function of temperature for the Er:SiN$_x$ sample with a refractive index 2.08 at 1.54 μm. In order to quantitatively analyze the temperature dependence of the Er lifetime, we used the following model to fit the data using (1):

$$\tau = \frac{1}{W_{T=0} + W_B \exp[(-E_A/kT)} \tag{1}$$

where $W_{T=0}$ is the decay rate at $T = 0$ and independent of temperature, E_A is the activation energy and W_B is the rate constant. From the best fit of the experimental data we found $E_A = 6.3$ meV. This demonstrates the existence of nonradiative trap states above Er $^4I_{13/2}$ level. The measured Er lifetimes at 4 and 300 K were 3.90 and 1.39 ms, respectively [Fig. 14(b), inset].

Fig. 14(a) displays the temperature dependence of Er I_{PL} at 1.54 μm of Er:SiN$_x$ sample in an Arrhenius plot. The PL spectra of the sample measured at 4 and 300 K are shown in the inset of the Fig. 14(a). The Er PL spectrum measured at 4 K demonstrates the overall quenching of the Er emission along with a sizeable reduction of the Er emission line shape, expected for phonon coupled inhomogeneously broadened transitions [56].

We point out that increasing temperature not only results in the reduction of PL quantum efficiency, as shown in Fig. 14(b), but can also affect the excitation rate of Er, and both the effects contribute to the temperature dependence of the Er PL intensity. This can be quantitatively understood by (2), which is generally

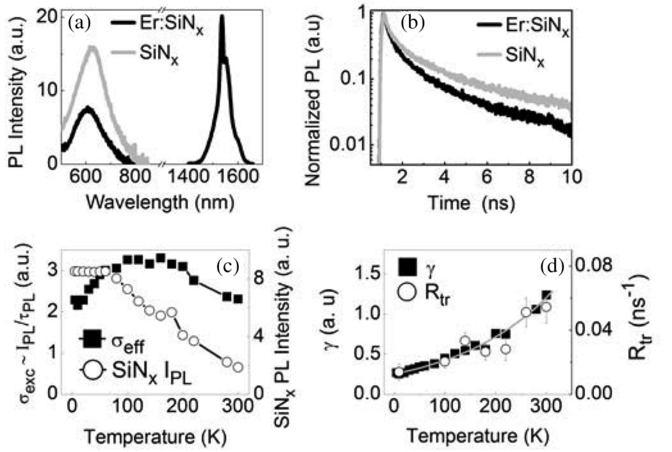

Fig. 15. (a) Visible PL spectrum at room temperature for stoichiometric SiN$_x$ samples doped and undoped with Er. (b) PL decay traces of the same sampled in (a). (c) Temperature dependence of the effective excitation cross section σ_{eff} (square) of Er in the sample with refractive 2.03 and SiN$_x$ integrated PL intensity (circle). (d) Coupling coefficient γ and transfer rate R_{tr} between SiN$_x$ and Er using two independent methods as described in the text. Samples are ~350 nm thick. Solid line is shown as a guide to the eye.

valid under weak excitation conditions

$$\frac{I_{\mathrm{PL}}(T)}{\tau(T)} \propto \sigma_{\mathrm{exc}}(T)\frac{\phi}{\tau_r}\,[N_{\mathrm{Er}}] \tag{2}$$

where σ_{exc} is the excitation cross section, ϕ is the photon flux and $[N_{\mathrm{Er}}]$ is the optically active Er concentration and τ_r is the radiative rate. Since ϕ is independent of temperature and we assuming the same for $[N_{\mathrm{Er}}]$ and τ_r, the temperature dependence of σ_{exc} can be obtained by measuring the ratio $I_{\mathrm{PL}}/\tau_{\mathrm{PL}}$, which is shown in Fig. 15(c). We see that σ_{exc} first increases until ~150 K then decreases. This interesting phenomenon deserves more investigation. In particular, the bell shape temperature behavior of σ_{exc} points toward a competition between donor concentration and coupling strength at different temperatures. This behavior can be quantitatively understood by remembering that, under weak excitation conditions, $\sigma_{\mathrm{exc}}(T) = \sigma_{\mathrm{Er}} + n_b(\phi, T)\gamma(T)/\phi$, where σ_{Er} is the excitation cross section of Er by direct absorption and can be neglected, ϕ is the temperature independent photon flux, n_b is the excited state population of the sensitizer (the SiN$_x$ matrix) and γ is the fundamental coupling coefficient between the sensitizer and Er. Since n_b is proportional to the PL intensity of the SiN$_x$ matrix, we can extract the temperature dependent coupling coefficient γ by considering the ratio $\sigma_{\mathrm{exc}}(T)/n_b(T)$. This ratio, which is proportional to γ, is plotted in Fig. 15(d) for different temperatures. The results demonstrate that the strength of the energy transfer increases with temperature and it is, therefore, a phonon-assisted transfer process. This conclusion can be confirmed by independently measuring the energy transfer rate to Er by time-resolved measurements at different temperatures. In order to perform this analysis, a pair of SiN$_x$ samples containing the same excess Si ($n \sim 2.03$) but doped (Er:SiN$_x$) and undoped (SiN$_x$) with Er were fabricated. The SiN$_x$ visible emission and Er I_{PL} at 300 K of the doped and undoped samples are shown in Fig. 15(a). The visible PL decay traces of the samples are shown in the inset of the figure for comparison. The reduction in the PL intensity and the shortening of the visible emission lifetime for the Er-doped sample allows to directly measure the energy transfer rate for samples with low Er concentration (~0.4%) [34]. The transfer rate R_{tr} can be estimated at any temperature, under weak pumping conditions, by the simple expression $1/\tau_d = 1/\tau_{ud} + R_{\mathrm{tr}}$ where τ_d and τ_{ud} are the decay times for Er-doped and undoped SiN$_x$ [26], [31]. Since the transfer rate equals the product of γ and the optically active Er concentration, which is assumed to be temperature independent, the temperature dependence of the transfer rate is the same as the temperature dependence of γ. We verified this assumption by directly measuring the energy transfer rate to Er at different temperatures from 4 to 300 K. The results are plotted in Fig. 15(d), and they demonstrate by two independent methods that the energy coupling coefficient γ strongly increases with temperature.

This analysis supports phonon-mediated energy transfer and demonstrates the competition between the increasing energy transfer rate and the decreasing density of excited sensitizers with temperature.

The strong temperature dependence of this energy transfer process suggests the possibility of thermally assisted tunneling of photo-excited carriers from localized states within the band tails of the amorphous SiN$_x$ matrix to the proximity of Er ions, with subsequent Er excitation by short-range coupling. The high density of band-tail states could account for the nanosecond-fast energy transfer time measured in Er:SiN$_x$, which is almost three orders of magnitude faster compared to traditional Er-doped Si-rich oxide systems.

VI. CONCLUSION

In this paper, we have shown our results on the structural and optical properties of light-emitting SiN$_x$-based samples fabricated by reactive sputtering. In particular, we have shown that visible light emission in amorphous SiN$_x$ materials originate from the radiative recombination of trapped carriers in the band-tails, which are involved in the excitation of Er ions by a non-resonant, phonon-mediated energy transfer process. In addition, we have presented a systematic optimization of the sensitized 1.54 μm Er emission in Er-doped SiN$_x$ films of different Si concentrations and annealed at different temperatures. Finally, we discussed the role of excess Si in the excitation/de-excitation processes of Er ions and we measured the temperature dependence of the energy transfer process which results in broad band, nanosecond-fast excitation of Er ions in SiN$_x$. The engineering of Er-doped amorphous SiN$_x$ materials with efficient and millisecond-long 1.54 μm Er emission has a large potential for the fabrication of optically active photonic devices based on the Si technology.

ACKNOWLEDGMENT

The authors would like to thank Prof. T. D. Moustakas for insightful discussions on the radiative physics of amorphous materials.

REFERENCES

[1] L. Pavesi, S. Gaponenko, and L. Dal Negro, *Towards the First Silicon Laser*, vol. 93. Dordrecht, The Netherlands: Kluwer, 2003.

[2] M. Lipson, "Guiding, modulating, and emitting light on silicon—Challenges and opportunities," *J. Lightw. Technol.*, vol. 23, no. 12, pp. 4222–4238, Dec. 2005.

[3] D. J. Lockwood and L. Pavesi, *Silicon Photonics*. Berlin, Germany: Springer-Verlag, 2004.

[4] N. Daldosso, M. Luppi, S. Ossicini, E. Degoli, R. Magri, G. Dalba, P. Fornasini, R. Grisenti, F. Rocca, L. Pavesi, S. Boninelli, F. Priolo, C. Spinella, and F. Iacona, "Role of the interface region on the optoelectronic properties of silicon nanocrystals embedded in SiO$_2$," *Phys. Rev. B*, vol. 68, pp. 85327–85327, 2003.

[5] L. T. Canham, "Silicon quantum wire array fabrication by electrochemical and chemical dissolution of wafers," *Appl. Phys. Lett.*, vol. 57, pp. 1046–1048, 1990.

[6] O. Boyraz and B. Jalali, "Demonstration of a silicon Raman laser," *Opt. Exp.*, vol. 12, pp. 5269–5273, 2004.

[7] H. S. Rong, A. S. Liu, R. Jones, O. Cohen, D. Hak, R. Nicolaescu, A. Fang, and M. Paniccia, "An all-silicon Raman laser," *Nature*, vol. 433, pp. 292–294, 2005.

[8] L. Pavesi, L. Dal Negro, C. Mazzoleni, G. Franzo, and F. Priolo, "Optical gain in silicon nanocrystals," *Nature*, vol. 408, pp. 440–444, 2000.

[9] J. Liu, X. Sun, D. Pan, X. Wang, L. C. Kimerling, T. L. Koch, and J. Michel, "Tensile-strained, n-type Ge as a gain medium for monolithic laser integration on Si," *Opt. Exp.*, vol. 15, pp. 11272–11277, 2007.

[10] K. D. Hirschman, L. Tsybeskov, S. P. Duttagupta, and P. M. Fauchet, "Silicon-based visible light-emitting devices integrated into microelectronic circuits," *Nature*, vol. 384, pp. 338–341, 1996.

[11] R. J. Walters, G. I. Bourianoff, and H. A. Atwater, "Field-effect electroluminescence in silicon nanocrystals," *Nat. Mater.*, vol. 4, pp. 143–146, 2005.

[12] H. S. Rong, R. Jones, A. S. Liu, O. Cohen, D. Hak, A. Fang, and M. Paniccia, "A continuous-wave Raman silicon laser," *Nature*, vol. 433, pp. 725–728, 2005.

[13] G. Franzo, A. Irrera, E. C. Moreira, M. Miritello, F. Iacona, D. Sanfilippo, G. Di Stefano, P. G. Fallica, and F. Priolo, "Electroluminescence of silicon nanocrystals in MOS structures," *Appl. Phys. A – Mater. Sci. Process.*, vol. 74, pp. 1–5, 2002.

[14] F. Iacona, D. Pacifici, A. Irrera, M. Miritello, G. Franzo, F. Priolo, D. Sanfilippo, G. Di Stefano, and P. G. Fallica, "Electroluminescence at 1.54 mu m in Er-doped Si nanocluster-based devices," *Appl. Phys. Lett.*, vol. 81, pp. 3242–3244, 2002.

[15] A. S. Liu, R. Jones, L. Liao, D. Samara-Rubio, D. Rubin, O. Cohen, R. Nicolaescu, and M. Paniccia, "A high-speed silicon optical modulator based on a metal-oxide-semiconductor capacitor," *Nature*, vol. 427, pp. 615–618, 2004.

[16] V. R. Almeida, C. A. Barrios, R. R. Panepucci, and M. Lipson, "All-optical control of light on a silicon chip," *Nature*, vol. 431, pp. 1081–1084, 2004.

[17] O. I. Dosunmu, D. D. Cannon, M. K. Emsley, B. Ghyselen, J. F. Liu, L. C. Kimerling, and M. S. Unlu, "Resonant cavity enhanced Ge photodetectors for 1550 nm operation on reflecting Si substrates," *IEEE J. Sel. Topics Quantum Electron.*, vol. 10, no. 4, pp. 694–701, Jul./Aug. 2004.

[18] M. Loncar, D. Nedeljkovic, T. Doll, J. Vuckovic, A. Scherer, and T. P. Pearsall, "Waveguiding in planar photonic crystals," *Appl. Phys. Lett.*, vol. 77, pp. 1937–1939, 2000.

[19] M. Makarova, V. Sih, J. Warga, R. Li, L. Dal Negro, and J. Vuckovic, "Enhanced light emission in photonic crystal nanocavities with Erbium-doped silicon nanocrystals," *Appl. Phys. Lett.*, vol. 92, pp. 161107-1–161107-3, 2008.

[20] G. Franzo, V. Vinciguerra, and F. Priolo, "The excitation mechanism of rare-earth ions in silicon nanocrystals," *Appl. Phys. A: Mater. Sci. Process.*, vol. 69, pp. 3–12, 1999.

[21] M. Fujii, M. Yoshida, Y. Kanzawa, S. Hayashi, and K. Yamamoto, "1.54 μm photoluminescence of Er^{3+} doped into SiO2 films containing Si nanocrystals: Evidence for energy transfer from Si nanocrystals to Er^{3+}," *Appl. Phys. Lett.*, vol. 71, pp. 1198–1200, 1997.

[22] M. Wojdak, M. Klik, M. Forcales, O. B. Gusev, T. Gregorkiewicz, D. Pacifici, G. Franzo, F. Priolo, and F. Iacona, "Sensitization of Er luminescence by Si nanoclusters," *Phys. Rev. B*, vol. 69, pp. 233315-1–233315-4, 2004.

[23] M. Fujii, M. Yoshida, S. Hayashi, and K. Yamamoto, "Photoluminescence from SiO$_2$ films containing Si nanocrystals and Er: Effects of nanocrystalline size on the photoluminescence efficiency of Er^{3+}," *J. Appl. Phys.*, vol. 84, pp. 4525–4531, 1998.

[24] D. Pacifici, G. Franzo, F. Priolo, F. Iacona, and L. Dal Negro, "Modeling and perspectives of the Si nanocrystals-Er interaction for optical amplification," *Phys. Rev. B*, vol. 67, pp. 245301.1–245301.13, 2003.

[25] L. Dal Negro, S. Hamel, N. Zaitseva, J. H. Yi, A. Williamson, M. Stolfi, J. Michel, G. Galli, and L. C. Kimerling, "Synthesis, characterization, and modeling of nitrogen-passivated colloidal and thin film silicon nanocrystals," *IEEE J. Sel. Topics Quantum Electron.*, vol. 12, no. 6, pp. 1151–1163, Nov./Dec. 2006.

[26] L. Dal Negro, R. Li, J. Warga, and S. N. Basu, "Sensitized erbium emission from silicon-rich nitride/silicon superlattice structures," *Appl. Phys. Lett.*, vol. 92, pp. 181105-1–181105-3, 2008.

[27] L. Dal Negro, J. H. Yi, M. Hiltunen, J. Michel, L. C. Kimerling, S. Hamel, A. J. Williamson, G. Galli, T. W. F. Chang, V. Sukhovatkin, and E. H. Sargent, "Light-emitting silicon-rich nitride systems and photonic structures," *J. Exp. Nanosci.*, vol. 1, pp. 29–50, 2006.

[28] L. Dal Negro, J. H. Yi, J. Michel, L. C. Kimerling, T. W. F. Chang, V. Sukhovatkin, and E. H. Sargent, "Light emission efficiency and dynamics in silicon-rich silicon nitride films," *Appl. Phys. Lett.*, vol. 88, pp. 183103-1–183103-3, 2006.

[29] L. Dal Negro, J. H. Yi, J. Michel, L. C. Kimerling, S. Hamel, A. Williamson, and G. Galli, "Light-emitting silicon nanocrystals and photonic structures in silicon nitride," *IEEE J. Sel. Topics Quantum Electron.*, vol. 12, no. 6, pp. 1628–1635, Nov./Dec. 2006.

[30] L. Dal Negro, R. Li, J. Warga, S. Yerci, S. Basu, S. Hamel, and G. Galli, "Light emission from silicon rich nitride structures," in *Silicon Nanophotonics: Basic Principles, Present Status and Perspectives*, L. Khriachtchev, Ed. Singapore: World Scientific, 2008.

[31] R. Li, J. R. Schneck, J. Warga, L. D. Ziegler, and L. Dal Negro, "Carrier dynamics and erbium sensitization in silicon-rich nitride nanocrystals," *Appl. Phys. Lett.*, vol. 93, pp. 091119-1–091119-3, 2008.

[32] J. Warga, R. Li, S. N. Basu, and L. Dal Negro, "Electroluminescence from silicon-rich nitride/silicon superlattice structures," *Appl. Phys. Lett.*, vol. 93, pp. 151116-1–151116-3, 2008.

[33] G. Y. Sung, N. M. Park, J. H. Shin, K. H. Kim, T. Y. Kim, K. S. Cho, and C. Huh, "Physics and device structures of highly efficient silicon quantum dots based silicon nitride light-emitting diodes," *IEEE J. Sel. Topics Quantum Electron.*, vol. 12, no. 6, pp. 1545–1555, Nov./Dec. 2006.

[34] S. Yerci, R. Li, S. O. Kucheyev, T. van Buuren, S. N. Basu, and L. Dal Negro, "Energy transfer and 1.54 μm emission in amorphous silicon nitride films," *Appl. Phys. Lett.*, vol. 95, pp. 0311107-1–0311107-3, 2009.

[35] R. Li, S. Yerci, and L. Dal Negro, "Temperature dependence of the energy transfer from amorphous Silicon nitride to Er ions," *Appl. Phys. Lett.*, vol. 95, pp. 041111-1–041111-3, 2009.

[36] A. Polman, "Erbium implanted thin film photonic materials," *J. Appl. Phys.*, vol. 82, pp. 1–39, 1997.

[37] L. R. Doolittle, "Algorithms for the rapid simulation of Rutherford Backscattering spectra," *Nucl. Instrum. Methods Phys. Res. Sect. B-Beam Interact. Mater. Atoms.*, vol. 9, pp. 344–351, 1985.

[38] J. R. I. Lee and T. van Buuren, personal communication, May 2009.

[39] B. S. Sahu, O. P. Agnihotri, S. C. Jain, R. Mertens, and I. Kato, "Influence of hydrogen on losses in silicon oxynitride planar optical waveguides," *Semicond. Sci. Technol.*, vol. 15, pp. L11–L14, 2000.

[40] K. M. Mikhail Baklanov and M. Green, *Dielectric Films for Advanced Microelectronics* (Wiley Series in Materials for Electronic & Optoelectronic Applications), 1st ed. New York: Wiley, Apr. 6, 2007.

[41] F. Giorgis, P. Mandracci, L. Dal Negro, C. Mazzoleni, and L. Pavesi, "Optical absorption and luminescence properties of wide-band gap amorphous silicon based alloys," *J. Non-Crystalline Solids*, vol. 266, pp. 588–592, 2000.

[42] F. Giorgis, C. Vinegoni, and L. Pavesi, "Optical absorption and photoluminescence properties of alpha-Si$_{1\text{-x}}$N$_\text{x}$: H films deposited by plasma-enhanced CVD," *Phys. Rev. B*, vol. 61, pp. 4693–4698, 2000.

[43] H. G. Tompkins, R. B. Gregory, P. W. Deal, and S. M. Smith, "Analysis of silicon oxynitrides with spectroscopic ellipsometry and Auger spectroscopy, compared to analyses by Rutherford backscattering spectrometry and Fourier transform infrared spectroscopy," *J. Vacuum Sci. Technol. A: Vacuum, Surfaces, Films*, vol. 17, pp. 391–397, 1999.

[44] H. Kato, N. Kashio, Y. Ohki, K. S. Seol, and T. Noma, "Band-tail photoluminescence in hydrogenated amorphous silicon oxynitride and silicon nitride films," *J. Appl. Phys.*, vol. 93, pp. 239–244, 2003.

[45] F. Giorgis, C. F. Pirri, C. Vinegoni, and L. Pavesi, "Luminescence processes in amorphous hydrogenated silicon-nitride nanometric multilayers," *Phys. Rev. B*, vol. 60, pp. 11572–11576, 1999.

[46] M. Wang, J. Huang, Z. Yuan, A. Anopchenko, D. Li, D. Yang, and L. Pavesi, "Light emission properties and mechanism of low-temperature

prepared amorphous SiN_x films. II. Defect states electroluminescence," *J. Appl. Phys.*, vol. 104, pp. 083505-1–083505-4, 2008.

[47] F. Boulitrop and D. J. Dunstan, "Phonon interactions in the tail states of alpha-Si-H," *Phys. Rev. B*, vol. 28, pp. 5923–5929, 1983.

[48] D. J. Dunstan and F. Boulitrop, "Photoluminescence in hydrogenated amorphous-silicon," *Phys. Rev. B*, vol. 30, pp. 5945–5957, 1984.

[49] R. A. Street, "Luminescence in amorphous semiconductors," *Adv. Phys.*, vol. 25, pp. 397–453, 1976.

[50] W. C. Ding, D. Hu, J. Zheng, P. Chen, B. W. Cheng, J. Z. Yu, and Q. M. Wang, "Strong visible and infrared photoluminescence from Er-implanted silicon nitride films," *J. Phys. D – Appl. Phys.*, vol. 41, pp. 135101-1–135101-4, 2008.

[51] M. Fujii, K. Imakita, K. Watanabe, and S. Hayashi, "Coexistence of two different energy transfer processes in SiO_2 films containing Si nanocrystals and Er," *J. Appl. Phys.*, vol. 95, pp. 272–280, 2004.

[52] K. Watanabe, M. Fujii, and S. Hayashi, "Resonant excitation of Er3+ by the energy transfer from Si nanocrystals," *J. Appl. Phys.*, vol. 90, pp. 4761–4767, 2001.

[53] O. Savchyn, R. M. Todi, K. R. Coffey, and P. G. Kik, "Multilevel sensitization of Er^{3+} in low-temperature-annealed silicon-rich SiO[sub 2]," *Appl. Phys. Lett.*, vol. 93, pp. 233120-1–233120-3, 2008.

[54] F. Priolo, G. Franzo, D. Pacifici, V. Vinciguerra, F. Iacona, and A. Irrera, "Role of the energy transfer in the optical properties of undoped and Er-doped interacting Si nanocrystals," *J. Appl. Phys.*, vol. 89, pp. 264–272, 2001.

[55] A. Polman, D. C. Jacobson, D. J. Eaglesham, R. C. Kistler, and J. M. Poate, "Optical doping of wave-guide materials by Mev Er implantation," *J. Appl. Phys.*, vol. 70, pp. 3778–3784, 1991.

[56] P. C. Becker, N. A. Olsson, and J. R. Simpson, *Erbium-Doped Fiber Amplifiers—Fundamentals and Technology*. San Diego, CA: Academic, 1999.

Selçuk Yerci (S'10) received the B.S. and M.S. degrees, both in physics, from the Middle East Technical University, Ankara, Turkey, in 2004 and 2007, respectively. He is currently working toward the Ph.D. degree in electrical engineering in the Department of Electrical and Computer Engineering and Photonics Center, Boston University , Boston, MA.

His research interests include fabrication, structural, optical, and electrical characterization of optoelectronic materials based on silicon nitride for monolithic nanophotonic light emitting devices.

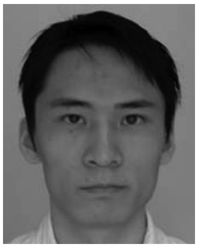

Rui Li received the B.S. degree in photonic science and technology from Sun Yat-Sen University, Guangzhou, China, in 2005. He is currently working toward the Ph.D. degree in electrical engineering in the Department of Electrical and Computer Engineering and Photonics Center, Boston University, Boston, MA.

His research interests include linear and nonlinear optical properties of amorphous silicon nitride, Er sensitization in amorphous silicon nitride, simulation and fabrication of waveguide and resonant photonic structures.

Sergei O. Kucheyev received the Ph.D. degree in physical sciences from the Australian National University, Canberra, Australia, in 2002.

He has been with the Lawrence Livermore National Laboratory (LLNL), Livermore, CA, since 2002, where he is currently a Physicist and a Research Staff Member of the Nano-Scale Synthesis and Characterization Laboratory. He joined LLNL as a Lawrence Postdoctoral Fellow and subsequently became a Staff Scientist. His research interests include structure–property correlation in nanoporous, nanostructured materials, radiation effects in solids, and growth and properties of solid hydrogens. He is the author of more than 100 technical papers.

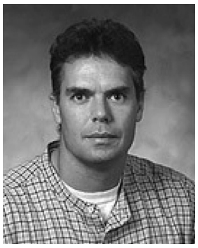

Tony van Buuren received the PhD. Degree in physics from the University of British Columbia, Vancouver, BC, Canada, in 1996.

He is currently with the Lawrence Livermore National Laboratory (LLNL), Livermore, CA, where he joined as a Postdoctoral Fellow in the Materials Science Division of the Chemistry and Materials Science Division, after completing the Ph.D. degree. In 1998, he became a Staff Scientist, and in 2007 became the Group Leader of the Nanoscale Materials Science and Technology Group of the Physical and Life Science Directorate, LLNL. His research interests include nanomaterials characterization using synchrotron radiation, and projects involving electronic and surface structure measurements of highly porous materials and membranes and group IV nanomaterials. He is the author and coauthor of more than 90 technical papers.

Soumendra N. Basu received the Ph.D. degree in materials science and engineering from Massachusetts Institute of Technology, Cambridge, MA, in 1989.

He was a Postdoctoral Research Associate at Los Alamos National Laboratory, Los Alamos, NM, prior to joining Boston University, Boston, MA, in 1990. He is the currently the Associate Division Head of the Division of Materials Science and Engineering and a Professor of Mechanical Engineering with the Boston University. His research interests include characterization of structure and phase transformations in materials using electron microscopy techniques, thermal barrier and environmental barrier coatings for gas turbine and fuel cell applications, thin films for photonic, electronic and superconducting applications, environmental degradation of materials at elevated temperatures, structure and stability of interfaces, and materials for clean energy conversion. He is the author of more than 100 technical papers, and has been on the Organizing/International Advisory Committees of several international conferences.

Luca Dal Negro received both the Laurea (*summa cum laude*) degree in physics, in 1999, and the Ph.D. degree in semiconductor physics from the University of Trento, Trento, Italy, in 2003.

In 2003, he joined Massachusetts Institute of Technology, Cambridge, as a Postdoctoral Associate. Since January 2006, he is an Assistant Professor in the Department of Electrical and Computer Engineering, Boston University, Boston, MA, and a Member of the Photonics Center. He manages and conducts research projects on silicon-based materials, devices and photonic structures. His current research interests include optical spectroscopy of nanostructures, complex photonic media, and nanoplasmonics. He is the author and coauthor of more than 80 technical papers.